MSWI bottom ash used as basement at two pilot-scale roads: Comparison of leachate chemistry and reactive transport modeling

Laurent De Windt, David Dabo, Sofia Lidelöw, Rabia Badreddine, Anders Lagerkvist

MSWI bottom ash used as basement at two pilot-scale roads: comparison of leachate chemistry and reactive transport modeling

Laurent De Windt[a,*], David Dabo[a,b], Sofia Lidelöw[c], Rabia Badreddine[b], Anders Lagerkvist[c]

[a] Ecole des Mines de Paris – Mines ParisTech, Geosciences Dept., 77305 Fontainebleau Cédex, France.

[b] INERIS, Wastes and Contaminated Sites Unit, 60550 Verneuil-en-Halatte, France.

[c] Luleå University of Technology, Division of Waste Science and Technology, SE-971 87 Luleå, Sweden.

* Corresponding author: laurent.dewindt@mines-paristech.fr, phone: +33-1-64.69.49.42, fax: +33-1-64.69.47.13, Ecole des Mines de Paris, Geosciences Dept., 35 Rue St-Honoré, 77305 Fontainebleau Cédex, France.

Abstract

The recycling of municipal solid waste incineration bottom ash as aggregates for road basement requires assessing the long-term evolution of leachate chemistry. The Dåva (Sweden) and Hérouville (France) pilot-scale roads were monitored during 6 and 10 years, respectively. Calculated saturation indices were combined to batch test modeling to set a simplified geochemical model of the bottom ash materials. A common reactive transport model was then applied to both sites. At Hérouville, pH and the concentration of most elements quickly drop during the first two years to reach a set of minimum values over 10 years. The decrease is less pronounced at Dåva. The evolution of pH and major element concentrations are fairly well related to the following pH-buffering sequence: portlandite, C-S-H phases or pseudo-wollastonite and, finally, calcite in equilibrium with atmospheric CO_2. $Al(OH)_3$, barite, ettringite and monohydrocalcite may also control leachate chemistry. Cu release is correctly modeled by DOM complexation and tenorite equilibrium. Temperature has no significant effect on the modeling of leachate chemistry in the range 5–30 °C, except at high pH. Effects at road edges and roadside slopes are important for the release of the less reactive elements and, possibly, for carbonation processes.

Keywords

bottom ash, environmental impact, geochemical modeling, trace metal, waste recycling

1. Introduction

The recycling of municipal solid waste incineration bottom ash (MSWI BA), as aggregates for road and car-park construction, may impact the environment - both soil and water resources - by releasing salts and heavy metals into the leachates (e.g. Kosson et al., 1996). Therefore, characterizing the long-term evolution of the leachate chemistry is an important facet of the environmental impact assessment of such reuse scenarios. Recently, in complement to a large body of data acquired with batch and column tests, a few reliable field data have been acquired in large scale experiments for several years (Åberg et al., 2006; Flyhammar and Bendz, 2006; Hjelmar et al., 2007; Lidelöw and Lagerkvist, 2007; Dabo et al., 2009). The intrinsic mineralogical heterogeneity of MSWI BA, as well as the variability in the climatic events, especially the rainwater infiltration regime, complicates the interpretation of leachate chemistry.

Several geochemical modeling studies have been published to interpret leachate evolution from MSWI BA submitted to batch and column lab tests (e.g. Meima and Comans, 1997; Park and Batchelor, 2002; Astrup et al., 2006; Dijkstra et al., 2008; Hyks et al., 2009). By contrast, only a few modeling studies have been devoted to MSWI BA weathering occurring at pilot-scale applications, either in lysimeter cell (Guyonnet et al., 2008; Mostbauer and Lechner, 2006) or landfill (Johnson et al., 1999; Baranger et al., 2002). However, such situations substantially differ from a road basement configuration. Edge effects that are typical of road structures cannot be correctly reproduced for instance. To the authors' knowledge, only Apul et al. (2007) developed a reactive transport model relevant for road basements but the complexity of the chemical processes have been simplified to a set of K_d parameters.

This paper aims at presenting the results of modeling of leachate from two pilot-scale road basements containing MSWI BA: the Dåva site in Sweden (Lidelöw and Lagerkvist,

2007) and the Hérouville site in France (Dabo et al., 2009), monitored for 6 and 10 years, respectively. The comparison of these two sites that were developed independently helps to shed light on common processes, but also discrepancies, in view of rationalizing leachate emission. In the first part of the paper, calculated saturation indices and solubility diagrams are combined to batch test modeling to set a simplified geochemical model of the two bottom ash materials. The second part of this paper attempts to develop a reactive transport model applicable to field conditions. A reactive transport model can help to identify and discriminate between the main hydrodynamic and geochemical processes and can be an useful tool for environmental impact assessments. The pH-buffering processes, and their effect on the evolution of leachate chemistry (major elements and trace metals) over time, are more particularly investigated.

2. Pilot-site configuration, material properties and batch tests

2.1 Configuration of the pilot-sites

The Dåva experimental road was built during the summer of 2001 at the Dåva power plant in Umeå (Sweden) and was used mainly by trucks for transport of incineration residues. Fig. 1 provides for schematic representation of the site. The road is 7 m wide and 80 m long. A 0.4 m thick subbase layer of MSWI BA is covered by a 15 cm base layer of rock crushed rock (gravel) and a 10 cm thick asphalt layer. Uncovered roadside slopes were built with the same bottom ash without being covered by asphalt. The average yearly precipitation in the area was about 600 mm per year during the sampling period, of which 40–50% falls as snow.

The Hérouville test road was built in 1997 in the Parisian Region (France) and characterized by a low traffic, about 10 vehicles per day. As schematically shown in Fig. 1, the road is 4 m wide and 20 m long and contains a 25 cm thick subbase layer of MSWI BA covered by a 15 cm thick asphalt cover. A polyethylene drainage liner (geomembrane) is

located at the bottom of the subbase layer. The road is fully embedded in a cultivated loamy and sandy soil. The depth of the local aquifer varies seasonally, between 3 and 7 m beneath the road. The local average precipitation rate was about 700 mm/y for the 1998-2008 period. There was an initial leachate production due to discharge by gravity during the very first weeks. Next, leachate volume was fairly well correlated to local precipitation in terms of intensity and frequency (Dabo et al., 2009). Leachate production was most probably linked to preferential flows since the geomembrane did not completely cover the road sides or edges, allowing lateral water infiltration into the subbase layer.

The methodology of leachate monitoring and sampling are presented into details in Lidelöw and Lagerkvist (2007) for the Dåva site and in Dabo et al. (2009) for the Hérouville site. The Hérouville road was monitored in two stages, from 1997 to 2000, and then again in 2007 to evaluate leachate chemistry after 10 years of utilization. MSWI BA samples were also collected by drilling after 10 years in the road subbase at Hérouville.

[FIGURE 1]

2.2 MSWI bottom ashes

The Swedish MSWI BA originated from the Dåva power plant in Umeå (Sweden). The plant was mainly fueled with MSW and small fractions of sorted industrial wastes such as wood, rubber and plastic. The bottom ash was screened to remove magnetic material and particles greater than 50 mm, and then weathered outdoor in heaps for 6 months. Compared with composition ranges of MSWI BA (Jeong et al., 2005), the material contained relatively large amounts of Cu and Zn, but small amounts of Al.

The French MSWI BA came from a municipal waste incineration facility located in the Parisian Region. Compared to the Swedish ash, metallic aluminum was also removed

from the bottom ash in addition to magnetic materials and the storage was shorter (< 3 months) corresponding to a lower stage of MSWI BA maturation. Compared with others MSWI BA (Jeong et al., 2005), the French bottom ash had relatively large amounts of Al and heavy metals Cu, Pb and Zn but relatively low contents of As, Cd and Hg.

2.3 Batch leaching tests

The model of the initial mineralogy of MSWI BA was partly derived from a set of batch leaching tests. A compliance test was applied to the Dåva bottom ash, consisting in a two-stage batch test at L/S 2 for 6 h and subsequently L/S 8 for 18 h according to the European standard EN 12457-3. Prior to the test, the samples were crushed and sieved to a particle size 95 wt% < 4 mm. Contrarily to the standard test, the MSWI bottom ash of the Hérouville site was neither crushed nor dried to prevent as much as possible any chemical artifacts. The L/S ratio ranged from 1 to 100. The batch tests were performed during 48h with distilled water in an airtight device, to avoid carbonation, under permanent agitation. Distilled water was used as a leachant, i.e., the leaching pH was dictated by the material itself. The leaching tests of Hérouville were made in 2008 and that, therefore, the MSWI bottom ash did not strictly correspond to the material used for the test road construction in 1997. However, both bottom ashes came from the same incineration facility without any significant change in the bottom ash production but a slight evolution of municipal waste sorting.

3. Modeling approach and data

3.1 Reactive transport code and thermodynamic database

All the calculations were done with the reactive transport code HYTEC (van der Lee et al., 2003) that couples advective and diffusive transport of solutes to chemical reactions. The flow and transport module was based on the representative elementary volume (REV)

approach with finite volume calculation. The Davies model was used for activity correction with an ionic strength limit of 0.5 mol/L.

The MINTEQ thermodynamic database (version 3.12, Allison et al., 1990) was selected and enriched with additional data for cement phases, as reported in Table 1. Calcium silicate hydrate (C-S-H) phases formed during weathering of bottom ash are usually poorly crystallized phases (Speiser et al., 2000). The saturation indices was calculated for both crystalline and amorphous C-S-H phases. The former were nevertheless used in the calculations because their formation constants were known at different temperatures, which allowed for analyzing temperature dependency in the range 5–30 °C. The solid $Pb(OH)_2$ was considered as a simplified formulation of more complex hydrous phases formed at alkaline pH (see De Windt and Badreddine, 2007).

The dissolved organic matter (DOM) of MSWI BA is known to have a strong affinity for Cu. A simple model was used to simulate the complexation process. Fulvic acids were assumed to be the responsible ligands for Cu-binding and to constitute 15 wt.% of the measured dissolved organic carbon (DOC), according to van Zoemeren and Comans (2004). Since there is no specific model for metal-fulvic interaction implemented in HYTEC, EDTA (ethylene-diamine-tetra-acetic acid) was considered as a substitute for the fulvic fraction. This molecule, that holds carboxylic acid functional groups as fulvics, is also a strong Cu complexant. The thermodynamic constants for EDTA acid/base properties and Cu complexation were taken from the MINTEQ database.

[TABLE 1]

3.2 Solubility controlled modeling

One of the major difficulties encountered in the modeling of MSWI BA chemical reactivity is their wide-ranging mineralogical composition. They are composed of quenched glass and

relic glass (about 50% by weight), native metals (Al, Fe) and a broad spectra of minerals such as silicates (e.g. feldspars, gehlenite, pseudo-wollastonite, quartz), carbonates (e.g. calcite), sulfates (e.g. ettringite, gypsum), aluminum and iron (hydr)oxides (e.g. gibbsite, magnetite). Furthermore, a given trace element is distributed among several solid phases. A second reason of modeling complexity is that many primary minerals formed during combustion, as well as glassy phases formed during quenching, remain permanently under-saturated (i.e. thermodynamically not stable) under meteoric weathering conditions. For instance, gehlenite was found to be strongly under-saturated with respect to leachate whatever the pH (section 4.2). Therefore, modeling their long-term evolution requires kinetic parameters (e.g. intrinsic rate constant, specific surface distribution) that are specific to each type of phases and are generally unknown.

One way to (partially) manage this modeling complexity is to only consider those minerals characterized by fast kinetics of reaction (e.g. calcite, C-S-H, ettringite, portlandite) that have been identified in the abundant literature on MSWI BA. These minerals are usually the by-products of the hydrolysis of the primary oxides formed during waste combustion. The dissolution and precipitation of the selected solid phases, characterized by fast kinetics, were assumed to be at thermodynamic equilibrium in the subbase layers. However, as discussed throughout the paper, the control of leachate chemistry by the primary phase pseudo-wollastonite was also considered as a modeling option. Kinetic rate constants were published for wollastonite under alkaline pH conditions (Golubev et al., 2006). The mean data is about 10^{-9} mol/m^2/s at 25°C. Kinetics required to estimate reactive surfaces, but this probably neither corresponds to a fast or to a slow kinetics of dissolution at the time scale of interest (from day to week). By simplicity, thermodynamic equilibrium was also assumed for pseudo-wollastonite in the model.

A second and complementary modeling approach is to consider that the solubility of trace metals is also controlled by secondary phases without explicitly considering the dissolution of primary source-terms. Mineral depletion of trace elements, after which sorption processes would take over, is assumed not to take place within the time frame of the measurements. Solubility control by secondary phases is a common fact in natural environment and has been experimentally demonstrated in the field of MSWI BA (e.g. Piantone et al., 2004). The solubility controlling phase usually varies according to the solution chemistry (e.g. hydroxides at high pH vs. carbonates at neutral pH). Sorption on Al and Fe oxyhydroxides is another important controlling process for trace metals. However, this mechanism was not considered in the present study since the trace element concentrations were systematically fixed by one or several secondary minerals. In principle, trace element concentrations are over-estimated in a solubility-controlled approach based on pure phases. Taking into account sorption processes or solid solution formation would decrease the calculated concentrations.

3.3 Flow and transport parameters

The main objective of the pilot-sites was leachate sampling and the hydrodynamic properties of the road components were relatively poorly characterized. Only the hydraulic conductivity at water saturation of the ten-year old bottom ash was estimated at Hérouville after removal of the asphalt cover ($K_{sat} \sim 5x10^{-6}$ m/s). The same value was assumed for the Dåva bottom ash. The hydraulic conductivities of the sandy and gravel materials were taken from the literature (Guymon, 1994). The hydraulic conductivities of the asphalt covers (i.e. runoff on the pavement vs. infiltration) were then adjusted (Table 2) to fit the chloride release profiles, in the roadside slope and under the asphalt pavement, assuming that precipitations were distributed evenly over the year. Differences between the horizontal and vertical hydraulic

conductivity were neglected for all the layers of the road base. The presence of preferential flow paths within the subbase layer was not investigated. However, the asphalt cover of the Dåva and Hérouville roads did not present any effective cracks after 6 and 10 years, respectively. The preferential flow pathway along the geomembrane observed in the Hérouville pilot-site was simulated by setting a higher hydraulic conductivity at the bottom of the MSWI BA subbase. The calculations were performed under water saturated conditions. A detailed unsaturated modeling linked to daily precipitation data was more costly in terms of computer time and could not be compared to site data since the leachates were sampled every two weeks only.

[TABLE 2]

4. Mineralogical model of the MSWI bottom ash

The geochemical model of the MSWI BA was built on taking into account: i) ash mineralogy, determined on the basis of both mineralogical analysis (XRD and SEM) of the Hérouville ash (Dabo et al., 2009) and literature review, ii) calculated saturation indices for Dåva and Hérouville field leachates, and iii) batch test modeling.

4.1 Brief literature review of solubility controlling minerals

According to the literature (Johnson et al., 1999; Meima and Comans, 1999; Dijkstra et al., 2008), there are three main sequences controlling the leachate concentrations in major elements during MSWI BA weathering: i) portlandite and gypsum for fresh unweathered bottom ash with leachate pH greater than 12, ii) ettringite, gibbsite and gypsum for quenched bottom ash with pH close to 10.5, and iii) calcite in equilibrium with atmospheric carbon dioxide (CO_2) for carbonated bottom ash with pH close to 8 (the mineral formulae can be

found in Table 1). It is likely that other cement-type phases are also active with respect to pH in the range 10.5 – 12. Thaumasite can contribute to pH-buffering at pH around 10 (Mostbauer and Lechner, 2006). However, this phase is generally present at a low content in MSWI BA compared to other sulfates like gypsum or ettringite (Piantone et al., 2004). Friedel'salt (equivalent to hydrocalumite) represents the Cl pole of the AFm cement-type phases. Its high molar content in hydroxyl ions could buffer the pH of leachate in the alkaline domain. The potential role of C-S-H in the alkaline pH range is mentioned by several authors (Johnson et al., 1999; Speiser et al., 2000; Piantone et al., 2004). Regarding the primary phases, wollastonite is the most likely to control Si concentration. For instance, Bodénan et al. (2010) indicated that leachate of boiler ash from a MSW fluidized-bed incinerator was close to thermodynamic equilibrium with this phase. This controlling process was assessed as an option of the mineralogical model of bottom ash. Pseudo-Wollastonite, its low pressure polymorph, was considered to be more representative of the solid formation during incineration.

4.2 Saturation indices of leachates

Some insights into the chemical processes occurring in the two pilot-scale roads were investigated with the geochemical module of HYTEC (named CHESS) by calculating saturation index (SI) of leachate with respect to primary and secondary minerals as well as by comparing field data with stability domains of Al-SO_4 minerals. Due to uncertainties, leachate is assumed to be in thermodynamic equilibrium with respect to a given mineral if the SI of this mineral ranges between -0.5 and 0.5 log unit. A positive SI (super-saturation or over-saturation state) indicates that the given mineral may precipitate as a secondary mineral. A negative SI (under-saturation state) indicates that the given mineral is not stable with respect to leachate chemistry and may dissolve provided the mineral is effectively present in the

material. Table 3 tabulates SI calculated for a selection of representative leachates. The selected data are denoted by square symbols in Figs. 5-6-7-9 that report the evolution with time of major and trace element concentrations in the leachates (discussed in Section 5). At both sites, the pH of the selected leachates decreases with time. Their temperatures are around 18 °C at Hérouville and range from 8 to 24 °C at Dåva.

Gehlenite, pseudo-wollastonite and quartz are all primary minerals of MSWI bottom ash. Gehlenite is systematically not stable (under-saturated) with respect to all leachates. Pseudo-wollastonite is slightly supersaturated at alkaline pH but under-saturated (i.e. thermodynamically unstable) at neutral pH. The opposite is true for quartz. At neutral pH, leachates are not far from equilibrium with quartz (and slightly under-saturated with respect to chalcedony that is most likely to precipitate at low temperature).

Portlandite is close to equilibrium or the saturation point (SI = -0.3) with respect to the very early leachates at Hérouville, which is consistent with the highest pH measured on site (pH = 12.4). In the very first months, the SI of Friedel'salt are supersaturated with respect to the alkaline and Cl-enriched leachates. As indicated by strongly negative SI, it becomes quickly unstable (among others, due to Cl leaching) and should dissolve. The SI of ettringite are positive at pH $\geq$ 11, but strongly negative below pH 10. Ettringite precipitation is therefore likely during the first years, whereas dissolution should occur on the long term. Thaumasite can precipitate from the early alkaline leachates of Hérouville (SI ~ 3) but not at moderately alkaline to neutral pH. At Hérouville, all the C-S-H phases, either crystalline or amorphous, are clearly close to equilibrium at alkaline pH but strongly under-saturated at slightly alkaline to neutral pH. The higher the pH is, the higher the Ca/Si is. C-S-H 1.8 and 1.1 are supersaturated at pH 12.4, but only C-S-H 1.1 at pH 11.4. Tobermorite (Ca/Si = 0.8) is the only stable phase at pH 11.4. All C-S-H phases are significantly under-saturated at neutral pH conditions.

Gypsum is always under-saturated with respect to leachates, whatever the pH or temperature. At Hérouville, amorphous $Al(OH)_3$ and gibbsite are clearly under-saturated in the alkaline pH range 12.5 – 10.5 whereas the former is not far from equilibrium at neutral pH. At Dåva, gibbsite is supersaturated at all pH values while amorphous $Al(OH)_3$ is not far from equilibrium at pH ≤ 10.5. Calcite is close to saturation in the long term leachate of Hérouville (pH ~ 8) while systematically supersaturated (SI ~ 1) in any other leachates, especially at alkaline pH. The same conclusion have been recently drawn for alkaline leachates of a boiler ash from a MSW fluidized-bed incinerator (Bodénan et al., 2010).

At Dåva, barite is systematically close to equilibrium whatever the pH and temperature (whereas witherite is always under-saturated). Tenorite is supersaturated at alkaline pH and close to equilibrium (Hérouville) or under-saturated (Dåva) on the long term. Cu-hydroxide is close to equilibrium at pH ~ 11. The interaction between Cu and dissolved organic matter (DOM) was not taken into account in these SI calculations. The leachates are under-saturated with respect to any secondary Pb phases, whatever the pH, temperature or time; especially at Dåva. For instance, the leachate are significantly under-saturated with respect to cerussite (SI ≤ 2) and hydrocerussite (SI ≤ 7), in agreement with the study of Mostbauer and Lechner (2006). Pb-hydroxide makes exception since it is close to equilibrium in the alkaline domain during the first year.

[TABLE 3]

4.3 Plot of Al and SO_4 solubility diagrams

Plotting the leachate data on calculated Al and SO_4 solubility diagrams is a complementary tool for data analyzing. The diagrams were built with CHESS and the present database, for chemical conditions representative of leachate. Despite a recurrent under-saturation state, amorphous $Al(OH)_3$ formation is relatively well corroborated by the plot of field data on the

Al solubility diagram (Fig. 2). In particular, Al concentration is strongly correlated to pH in the range 10 – 6. It is worth noting that the Dåva field data match the ettringite solubility limits in both Al and SO_4 solubility diagrams fairly well. In agreement with SI calculation, the SO_4 field data are systematically below the gypsum solubility limit.

[FIGURE 2]

4.4 Batch test modeling and initial mineralogy

Fig. 3 shows the experimental and modeling data of batch tests applied to the Hérouville and Dåva MSWI bottom ashes. The mineralogical model was mainly derived from the tests related to the Hérouville ash. The evolution of pH with L/S is well reproduced by modeling (Fig. 3a). A few amount of portlandite was introduced in the initial mineralogy to simulate the highest pH values. C-S-H phases were then taken into account to model the subsequent evolution of pH and Ca concentration. In cement chemistry, to given pH of solution corresponds a given Ca/Si ratio of C-S-H (e.g. Blanc et al., 2010). Hillebrandite (Ca/Si = 2.0) was considered in the present case. Results of similar quality were, however, obtained when pseudo-wollastonite was substituted to hillebrandite. The normalized release Cl data are perfectly in a (horizontal) line, both experimentally and in the modeling (Fig. 3b). This is indicative of a conservative behavior or, equivalently, that pore water is the main source of Cl. On the opposite, the evolution of Ca and SO_4 release with L/S are representative of solubility controlling processes. The model fairly well simulates Ca release with L/S increase. For SO_4, the experiment/model agreement is satisfactory at L/S = 5, 10 and 100 but fail to simulate the lowest L/S. Considering a small amount of gypsum improved the modeling.

In order to reduce the number of fitted parameters, the modeling of DOM release behavior was also derived from batch test data (available for Hérouville only). As shown in Fig. 3b, the experimental values of COT slightly increases with L/S. COT release is thus not

fully conservative. Nevertheless, in a first approximation, pore water was assumed to the single source of DOM in the model. This initial value was derived from the batch test at L/S = 1, the most relevant for L/S in the basement (L/S ~ 0.2). The agreement between the measured and calculated leached Cu at L/S =10 is also clearly improved while considering Cu-DOM interactions (Fig. 3c); which "validates" the EDTA approximation discussed in Section 3.1. Fig. 3c shows the full batch data set at L/S = 10. Beside Cl and pH, which were adjusted to batch data, the model correctly matches the experimental data (Al excepted, with an underestimation of two orders of magnitude).

Table 4 gives the proportions in the raw MSWI BA of the reactive minerals of interest for the modeling. As discussed, halite, sylvite and portlandite contents were quantitatively derived from batch leaching tests. The content in C-S-H phase, or pseudo-wollastonite as a second option, was derived from the pH evolution with increasing L/S. The contents in calcite, ettringite and quartz were semi-quantitatively estimated from XRD analyses. C-S-H phases are considered as modeling analogues to simulate the pH transient stage in the range 12 – 10.5, though they themselves derived from the hydrolysis of primary alkaline phases. Trace metals were introduced as (hydr)oxide (Cu, Pb) at an arbitrary low content (0.1% by weight) though high enough to ensure that mineral depletion of trace elements did not to take place within the modeled time frame. The other solid phases that could possibly precipitate during the modeling of the system evolution are written in bold in Table 3.

For the Dåva bottom ash, the compliance batch test at L/S = 10 was only available. In a first approximation, the mineralogical set assumed for the Hérouville material was applied to the Dåva material. This makes sense for the potential secondary phases that may precipitate under the road conditions, which are not fundamentally different from the Hérouville site. This also partly justified for the initial mineralogy since MSWI BA described in the literature share many similarities. However, some specific adjustments were required. Firstly, halite and

sylvite contents were directly derived from batch test. Secondly, at the higher stage of maturation of the Dåva bottom ash corresponds a lower pH (pH = 11 instead of 12.3). This pH could be simulated assuming portlandite depletion and C-S-H of lower Ca/Si ratios. The best pH adjustment was obtained with tobermorite, although pH was underestimated by 0.5 pH unit (Fig. 3d). The mineralogical model of the Dåva MSWI BA is given in Table 4. Globally, the modeling of the batch test is satisfactory for most elements (including Al); excepted Pb that is overestimated by two orders of magnitude (Fig. 3d).

[TABLE 4 – FIGURE 3]

5. Leachate evolution and reactive transport modeling

5.1 Flow field

Fig. 1 shows the grids used in the reactive transport calculations and the location of the leachate collectors. A full cross section was required for modeling the Hérouville road due to the asymmetric location of the sampling system (at the right-hand side of the road), which generates a dissymmetric water flow. Half a cross section was sufficient for the symmetric Dåva road. The calculated water flow field is given in Fig. 4. At Dåva, the runoff at the surface of the pavement goes towards the ditch with a maximum water infiltration calculated for the uncovered slopes. This is in agreement with field measurement where the majority of leachate was produced in the roadside slopes. At Hérouville, modeling leads to runoff on the pavement and a moderate water infiltration at the road edges. The model also took into account the initial leachate production that occurred during the very first weeks due to water discharge by gravity. The infiltrated water at the road edges was further canalized by the geomembrane towards the collector. This artifact of the sampling system was correctly reproduced by the model.

[FIGURE 4]

5.2 Release of Cl, Na and DOC

Field data

Fig. 5 shows the evolution with time of the leachante concentrations of Cl, Na and DOC at the sampling points. At Hérouville, Ca and Na leachate concentrations are initially about 1000 mg/L and progressively decrease over time to reach a mean value of 100 mg/L after 10 years. The initial values are higher at Dåva, around 10 000 mg/L. Data scattering is more pronounced at Hérouville. Edge effects are important for Cl and Na releases. While the asphalt cover is a barrier against rainwater percolation through the bottom ash layer, Cl and Na release is much more pronounced in the uncovered slopes at Dåva or driven by lateral inflows at Hérouville. Lateral inputs have been theoretically assumed to be a major source of leachate production by different authors (Kosson et al., 1996; Apul et al., 2007). The increase of Cl concentrations after 5 years in the roadside slope at Dåva may be due to engineering works performed during this period.

At Hérouville, DOC leachate concentrations are about 1000 mg/L the first month and rapidly decrease over time to reach a mean value of 10 mg/L after 10 years. DOC distribution is scattered. At Dåva, DOC leachate concentrations are about 100 mg/L. The contrasted leaching between the roadside slope and under the pavement is noticeable, but field DOC concentrations decrease more slowly than the corresponding Cl and Na ones.

Modeling

Fig. 4 gives a 2D picture of the Cl plumes calculated after 3 years. Cl ions have been leached away at the edges and roadside slopes but preserved from leaching by the asphalt cover. The barrier effect of the geomembrane at Hérouville can also be noticed in the figure. Despite the simplified hydrodynamic modeling approach, the Cl field data are well fitted by the model

(Fig. 5); supporting the modeling assumption that Cl was non reactive (conservative) and mainly present in the initial pore water. Diffusion inside the bottom ash layer below the pavement is combined to weak lateral flows. Na release is closely related to Cl release which is demonstrated by the very good agreement between the field data and calculated curve (fitted on the chloride content only). However, the molal ratio Na/Cl that is initially close to unity increases over time progressively. This suggests another sources of Na release on the long-term, such as the slow dissolution of glassy particles.

In the modeling of the Hérouville site, the release of dissolved organic carbon (DOC) is similar to the release of dissolved chloride salts. The calculated data represent an upper limit to field data. Such an upper limit might validate the assumption that the main source of DOM is also the initial pore water of the MSWI bottom ash.

[FIGURE 5]

5.3 Evolution of pH with time

Field data

Fig. 6 shows the pH field data plotted as a function of time. The pH values are significantly more scattered than Cl concentrations. However, at Hérouville, pH clearly decreases over the first three years, starting with very alkaline pH (> 12), followed by an intermediate stage of moderately alkaline pH (11.5 – 9.5), to reach a long-term pH value of about 7.5. At Dåva, pH remains within the range 11.5 – 10.5 during the first 4 years but eventually drops to 8 in the roadside slopes. The permanently high pH of the leachate beneath the asphalt cover demonstrates that carbonation was hampered by limited infiltration and gas exchange and that microbial production of CO_2 can be neglected. Similarly, batch tests applied to ten-year old drilled core samples inside the subbase at Hérouville indicated that carbonation was still in progress (Dabo et al., 2009). A similar situation has also been reported in a 10-year old

asphalt road with steel slag of electric arc furnace (Suer et al., 2009). The slag from the pavement edge showed traces of carbonation and leaching processes, whereas the road centre material was nearly identical to fresh slag, in spite of an accessible particle structure.

Modeling

The two driving forces for the long-term evolution of the bottom ash chemistry considered in this modeling study are: i) the transport of dissolved species by rainwater infiltration (mostly at the edges) as well as diffusion (mostly inside the subbase layer), as introduced in the discussion of Cl release, and ii) the neutralization of alkalinity by reaction with carbon dioxide (CO_2), which might have a strong effect on ash mineralogy and on the pH evolution of leachates. Diffusion of gaseous CO_2 from the atmosphere into the road sides and basement can occur since the MSWI BA is not water saturated in reality. To a lesser extent, microbiological degradation (respiration) of the MSWI BA may also yield in situ production of CO_2 (Rendek et al., 2006).

At Hérouville, a preliminary calculation indicates that pH would remain constantly high (Fig. 6, "no CO_2" legend), in contrast with field data, if dissolved CO_2 in rainwater was considered as the only input of CO_2. The same conclusion can be drawn from the comparison of Ca field data and modeling (Fig. 7, "no CO_2" legend). Since gaseous diffusion cannot be modeled by HYTEC, the carbonation process was simulated through a permanent input of CO_2 to the system according to a zero order rate: $d[CO_2]/dt = k$. The rate constants k were adjusted to fit as best as possible the evolution of pH with time under Hérouville edge zones (which locations are specified in Fig. 1). Though a direct physical meaning cannot be assigned to this constant, the adjusted input rate was about 50 mmol/dm^3/y. The calculated pH profiles resulting from the progressive carbonation of MSWI BA is in better agreement with the field data. Note that the temperature of reference in the present discussion is 15 °C.

Temperature effect is further discussed in Section 6. The calculated profile constitutes an upper envelop of field data. In the modeling, the pH is buffered around 12.5 by portlandite equilibrium during the first months of leachate emission while this mineral is progressively leached out and carbonated according to the following reaction:

$$\text{portlandite} + H_2CO_3 \rightarrow \text{calcite} + 2\,H_2O \quad (1)$$

H_2CO_3 denotes the dissolved form of carbon dioxide. Decalcification of C-S-H of high Ca/Si ratio takes place once portlandite is fully depleted, buffering the pH in the range 12–10.5:

$$3\ \text{hillebrandite} + 3.5\,H_2CO_3 \rightarrow 3.5\ \text{calcite} + 0.5\ \text{tobermorite} + 4\,H_2O \quad (2)$$

An equivalent reaction can be associated to pseudo-wollastonite in the same pH domain:

$$CaSiO_3 + H_2CO_3 \rightarrow \text{calcite} + \text{quartz} + H_2O \quad (2bis)$$

In a third stage, the dissolution of C-S-H of low Ca/Si ratio, and to a lower extent ettringite, keeps pH in the range 10.5–9.5:

$$\text{tobermorite} + 5\,H_2CO_3 \rightarrow 5\ \text{calcite} + 6\ \text{quartz} + 10\,H_2O \quad (3)$$

$$\text{ettringite} + 3\,H_2CO_3 \rightarrow 3\ \text{calcite} + 3\ \text{gypsum} + 2\,Al(OH)_3(am) + 26\,H_2O \quad (4)$$

These reactions seem to have been active at least during the first two years at the Hérouville pilot-site. On the long term, equilibrium of calcite with atmospheric CO_2 pressure ($4x10^{-4}$ atm) buffers pH around 8 according to the following reaction:

$$\text{calcite} + H_2CO_3 \rightarrow Ca^{2+} + 2\,HCO_3^- \quad (5)$$

The mineralogical transformations controlling pH through reactions 1 to 4 are reported in Fig. 8. The amount of calcite, which is an end-product of reactions 1 – 4, increases from 10 to 13.5 wt% in the edges.

At Dåva, the best agreement of modeling with the field data was obtained without assuming an additional input of CO_2 beside rainwater content. However, the data measured after 6 y in the roadside were finely reproduced by fixing an atmospheric input rate of 50

mmol/dm^3/y approximately. C-S-H and ettringite carbonation is so completed after 6 years, leading to a pH around 8 in agreement with reaction 5.

[FIGURES 6 – 7 – 8]

5.4 Release of major elements

Field data

At Hérouville, leachate Ca concentrations decrease from 1000 mg/L to 100 mg/L during the first year and then remain constant. SO_4 concentrations are scattered around a mean value of 150 mg/L but show a slightly increasing trend on the long term. Al concentrations are low, ranging between 0.1 and 10 mg/L, and become even lower after 10 y. Si concentrations are more or less constant, around 5 mg/L. At Dåva, Al concentrations are one order of magnitude higher but eventually drop to a value similar to Hérouville once pH becomes neutral. The maximum Ca concentrations are also about 100 mg/L but many values are one order of magnitude smaller. SO_4 concentrations are characterized by a decreasing trend during the first year and a convergence to a range of values similar to Hérouville ones. Si concentrations are one order of magnitude lower than the values measured at Hérouville. CO_3 concentrations are relatively constant over time, around 10 mg/L.

Modeling

At Hérouville, the evolution with time of Ca leachate concentrations is in straight relation with pH-buffering, as shown in Fig. 7. Ca concentration is first controlled by portlandite dissolution, then C-S-H and ettringite dissolutions and, eventually, calcite solubility in equilibrium with atmospheric CO_2. The modeling results are in good agreement with the field data though systematically maximized. At Dåva, the modeling overestimates field data. Similar trends are obtained when the C-S-H phases are substituted by pseudo-wollastonite.

The evolution of SO_4 concentration is driven both by hydrodynamics and chemical processes. The early decrease during the first year at both sites is similar to Cl release. A soluble fraction ($CaSO_4$) is evacuated by water discharge and rainwater infiltration. The calculated SO_4 concentration is then controlled by ettringite, as long as the pH remains above 10, and by secondary gypsum when pH decreases to 8. The thermodynamic equilibrium approach produces step-like increase in SO_4 concentrations coupled to pH evolution. Ettringite dissolution yields gypsum and Al-hydroxide precipitation according to reaction 4, as shown in Fig. 8. At Hérouville, XRD analysis indicated ettringite depletion in the ten-year old samples contrarily to the fresh samples (Dabo et al., 2009). According to the SO_4 solubility diagrams of Fig. 2, SO_4 concentrations should be lower at high pH, in conjunction with ettringite equilibrium, but should increase when pH decreases during carbonation to reach gypsum saturation. This is roughly the case at Hérouville but not at Dåva.

The evolution with time of Al leachate concentrations is reported in Fig. 6. Constraining Al concentration by ettringite equilibrium is very sensitive to pH. At Hérouville, the model clearly fails to simulate field data with both ettringite or gibbsite Al control. This was already the case in the modeling of batch tests (Section 4.4). The theoretical very low concentrations calculated with ettringite may, in reality, be out-competed by the numerous secondary mineralogical transformations occurring at field. Moreover, Bodénan et al. (2010) reported important fluctuation of ettringite SI suggesting these phases did not reach equilibrium during leaching experiment applied to bottom ash from MSW fluidized-bed incinerator. At Dåva, the calculated concentrations may represent a lower limit to field data (equivalently with ettringite or gibbsite). When pH falls below 10, the precipitation of amorphous $Al(OH)_3$ decreases Al concentrations at both sites.

At Dåva, CO_3 solubility control by calcite underestimates by one order of magnitude field data at alkaline pH; the agreement being much better at neutral pH. Dijkstra et al. (2008)

modified the formation constant (logK) of calcite according to the generally observed calcite supersaturation in leachate from incineration residues. In the present case, the model nicely reproduces field data in the alkaline range when monohydrocalcite is substituted for calcite (in agreement with the study of Bodénan et al., 2010). CO_3 concentrations are better simulated with the calcite solubility control when the pH drop induced by CO_2 "atmospheric" input is taken into account at the Dåva roadside. At Hérouville, the calculated carbonate content of the leachate at neutral pH are under-estimated by a factor 3. This small discrepancy is related to the slight overestimation of both Ca concentration and pH by the model that induces a decrease of CO_3 through the solubility product of calcite.

At the most alkaline pH values (Hérouville site), the Si solubility control by C-S-H leads to a clear underestimation of field data. Likewise Al, this is induced by the corresponding high Ca concentrations and the thermodynamic equilibrium approach. Once pH and Ca concentration have sufficiently decreased, after 2 y, Si concentration become controlled by tobermorite and the model generates data much closer to field. The field data are correctly simulated over a wider pH range when pseudo-wollastonite is substituted for C-S-H phases. At neutral pH, Si concentrations are well reproduced by quartz (or chalcedony) solubility. At Dåva, tobermorite solubility leads to satisfactory results for Si over the full period; quartz becoming a possible controlling phase when pH drops to 8.

5.4 Release of Ba, Cu and Pb

Field data

Fig. 9 shows the evolution with time of Ba, Cu and Pb concentrations in the leachates at the sampling points (Ba was not measured at Hérouville). At Dåva, Ba leachate concentrations do not vary with time and remain within the range 0.02 – 0.1 mg/L. The mean concentration in the roadside slopes is slightly smaller than the mean concentration measured below the

asphalt cover. Cu leachate concentrations range from 10 to 0.05 mg/L. There is clear decrease of Cu concentration with time at Hérouville and the Dåva roadsides, which is most probably linked to the release of DOM (Fig. 5). The two sites differ significantly with respect to Pb leachate concentrations. The Hérouville site is characterized by a fast decrease over the first two years, from 5 to 0.01 mg/L; Pb leachate concentrations remaining relatively constant on the long term. Most of the Pb concentrations at Dåva are directly ≤ 0.01 mg/L without any obvious evolution with time.

Modeling

The agreement between field and calculated data is particularly good in the case of Ba. The modeling of Ba concentration is intrinsically linked to the modeling of SO_4 concentration through the solubility product of barite. The good agreement demonstrates the global consistency of the present model. However, on the contrary, any degradation of the quality of SO_4 modeling content will affect the quality of Ba modeling.

There is a good agreement between field and calculated Cu concentrations when the Cu-DOM interaction is taken into account in the model (Hérouville site only). Cu release is clearly driven by the combination of transport due to DOM complexation and tenorite equilibrium. It is worth mentioning that tenorite is always in equilibrium, even with respect to the initial leachates in which the apparent solubility is enhanced by DOM complexation. The theoretical curve represents an upper limit for field data, identically to DOC modeling (section 4.3). At Dåva, field data are not far from tenorite solubility on the long term when a substantial fraction of DOM has been leached out.

At Hérouville, the calculated Pb leachate concentrations are in reasonable agreement with field data. There is also a decrease of 2 orders of magnitude during the first two years, which is linked to pH evolution in the range 12.5 – 10 (at least in the model). While

carbonation progressively lowers pH, Pb solubility is successively controlled in the model by: $Pb(OH)_2(s)$ in the pH range 13 – 11, $Pb_2(OH)_3Cl$ in the range 11 – 9.5 and cerussite at pH < 9. Nevertheless, the model fails to reproduce the low Pb concentrations, either at neutral pH at Hérouville or for the full pH range at Dåva. This was already the case in the modeling of the compliance batch test (Section 4.4). Pb co-precipitation with calcite or sorption on Al-Fe-hydroxides have been observed in the Hérouville MSWI bottom ash (Dabo et al., 2008).

[FIGURE 9]

6. Water residence time and temperature effects

The scattering of leachate data may partly come from variations in water residence time depending on the precipitation regime. Indeed, considering in the model an annual rate of rainwater infiltration combined with a thermodynamic equilibrium is a source of uncertainty with respect to pH and element concentrations. Some of the precipitation events are more intense and lead to faster leachate transfers inside the road basement (e.g. Dabo et al., 2009). Fast transfers mean low residence times and, therefore, an incomplete dissolution of the solubility-controlling minerals (i.e. thermodynamic equilibrium is not reached). An improved modeling would, therefore, require a kinetic approach for the selected minerals despite their relatively fast kinetics. Field under-saturation may also result from dilution due to the mixing of MSWI BA leachate with rainwater flowing in preferential pathways.

To a lesser extent, seasonal variations of temperature may also produce data scattering. For that purpose, pH and element concentrations of the Hérouville leachates were calculated at 5, 15 and 30 °C (Fig. 3 and 6). The differences between the profiles are directly linked to the temperature-dependency of the thermodynamic equilibrium constants in the present modeling approach (i.e. potential catalyzing effects of temperature on microbial

kinetics are not analyzed here). Temperature effect on pH is effective for leachates in equilibrium with portlandite, pH decreases by one unit when temperature rises from 5 to 30° C. There is no significant temperature effect at slightly alkaline and neutral pH. Temperature effect on the leachate concentrations of major and trace elements is weak in the range 5–30° C, except for Pb whose solubility is strongly dependent on pH. Pb concentration decreases by one order of magnitude from 5 to 30° C at strongly alkaline pH; temperature effect is much weaker otherwise.

7. Conclusions

The comparison of leachate chemistry at the Hérouvile and Dåva pilot-scale roads helps to shed light on common processes, but also discrepancies, in view of rationalizing the leachate long-term evolution. Calculated saturation indices and solubility diagrams have been combined to batch test modeling to set a simplified geochemical model of the two bottom ash materials. A common reactive transport model has then been applied to both pilot-scale roads.

At Hérouville, pH and the concentration of most major and trace elements quickly drop during the first two years to asymptotically reach a set of minimum values over 10 years. The decrease is less pronounced at Dåva. The evolution of pH and major element concentrations are fairly well related to the following pH-buffering sequence: portlandite (Hérouville only), C-S-H or pseudo-wollastonite and, finally, calcite in equilibrium with atmospheric CO_2. $Al(OH)_3$, barite, ettringite, monohydrocalcite may also control leachate chemistry. Cu release is correctly modeled by DOM complexation and tenorite equilibrium. At Hérouville, Pb concentration decreases by two orders of magnitude in the pH range 12.5 – 10. The solubility-controlled approach fails to reproduce the lowest Pb concentrations, requiring sorption or co-precipitation modeling. Temperature has no significant effect on the modeling of the leachate chemistry in the range 5–30 °C, except at high pH. Effects at road

edges and roadside slopes have been show to be important for the release of the less reactive elements and, possibly, for carbonation processes driven by atmospheric CO_2 inputs.

The relevancy of the C-S-H/pseudo-wollastonite to simulate the pH transient stage in the range 12 – 10.5 should be further investigated experimentally. The reactive transport model may be an useful tool for environmental impact assessments, but this requires to take into account other potential contaminants. Further developments of HYTEC is needed for implementing existing gas transport models to better assess carbonation at field scale.

Acknowledgements

The authors thank Ivan Drouadaine from EUROVIA (France) for supporting leachate sampling and analyses at the Hérouville site. Three anonymous reviewers are also gratefully acknowledged for their detailed comments and fruitful suggestions.

References

Åberg, A., Kumpiene, J., Ecke, H., 2006. Evaluation and prediction of emissions from a road built with bottom ash from municipal solid waste incineration (MSWI), Sc. Total Environ. 355, 1-12.

Allison, J.D., Brown, D.S. Novo-Gradac, K. J., 1990. MINTEQA2/PRODEF2, A Geochemical Assessment Model for Environmental Systems: Version 3.0 User's Manual, U.S. Environ. Prot. Agency, Athens (USA).

Apul, D.S., Gardner, K.H., Eighmy, T.T., 2007. Modeling hydrology and reactive transport in roads : The effect of cracks, the edge, and contaminant properties, Waste Manage. 27, 1465-1475.

Astrup, T., Joris J. Dijkstra, J.J., Comans, R.N.J., van der Sloot, H.A., Christensen, T.H., 2006. Geochemical modeling of leaching from MSWI air-pollution-control residues, Environ. Sci. Technol. 40, 3551-3557.

Baranger, P., Azaroual, M., Freyssinet, P., Lanini, S., Piantone, P., 2002. Weathering of a MSW bottom ash heap: a modelling approach, Waste Manage. 22, 173-179.

Blanc, Ph., Bourbon, X., Lassin, A., Gaucher, E.C., 2010. Chemical model for cement-based materials: Temperature dependence of thermodynamic functions for nanocrystalline and crystalline C–S–H phases, Cement Concrete Res. 40, 851-866.

Bodénan, F., Guyonnet, D., Piantone, Blanc, P., 2010. Mineralogy and pore water chemistry of a boiler ash from a MSW fluidized-bed incinerator, Waste Manage. 30, 1280-1289.

Bothe, J., Brown, P., 2004. PhreeqC modeling of Friedel's salt equilibria at 23C. Cement Concret Res. 34, 1057-1063.

Dabo, D., Raimbault, L., Badreddine, R., Chaurand, P., Rose, J., De Windt, L., 2008. Characterisation of Glassy and Heterogeneous Cementing Phases of Municipal Solid

Waste of Incineration (MSWI) Bottom Ash, Australasian Institute of Mining and Metallurgy Publication Series , pp. 95-99.

Dabo, D., Badreddine, R., De Windt, L., Drouadaine , I., 2009. Ten-year chemical evolution of leachate and municipal solid waste incineration bottom ash used in a test road site, J. Hazard. Mater. 172, 904-913.

Damidot, D., Glasser, F.P., 1993. Thermodynamic investigation of the $CaO-Al_2O_3-CaSO_4-H_2O$ system at 25°C and the influence of Na_2O, Cement Concrete Res. 23, 221-238.

De Windt, L., Badreddine, R., 2007. Modelling of long-term dynamic leaching tests applied to solidified/stabilised waste, Waste Manage. 27, 1638-1647.

Dijkstra, J.J., Meeussen, J.C.L., Van der Sloot, H.A., Comans, R.N.J., 2008. A consistent geochemical modelling approach for the leaching and reactive transport of major and trace elements in MSWI bottom ash, Appl. Geochem. 23, 1544-1562.

Flyhammar, P., Bendz, D., 2006. Leaching of different elements from subbase layers of alternative aggregates in pavement constructions, J. Hazard. Mater. 137, 603-611.

Golubev, S.V., Pokrovsky, O.S., Schott, J., 2006. Experimental determination of the effect of dissolved CO2 on the dissolution kinetics of Mg and Ca silicates at 25°C. Chem. Geol. 217, 227-238.

Guymon G.L., 1994. Unsaturated zone hydrology, Prentice Hall Ed., Englewood Cliffs (USA).

Guyonnet, D., Bodénan, F., Brons-Laot, G., Burnol, A., Chateau, L., Crest, M., Méhu, J., Moszkowicz, P., Piantone, P., 2008. Multiple-scale dynamic leaching of a municipal solid waste incineration ash, Waste Manage. 28, 1963-1976.

Hjelmar, O., Holm, J., Crillesen, K., 2007. Utilisation of MSWI bottom ash as subbase in road construction : First results from a large-scale test site, J. Hazard. Mater. 139, 471-480.

Hyks, J., Astrup, T., Christensen, T.H., 2009. Leaching from MSWI bottom ash: Evaluation of non-equilibrium in column percolation experiments, Waste Manage. 29, 522-529.

Jeong, S.M., Osako, M., Kim, Y.J., 2005. Utilizing a database to interpret leaching characteristics of lead from bottom ash of municipal solid waste of incinerators, Waste Manage. 25, 694-701.

Johnson, C.A., Kaeppeli, M., Brandenberger, S., Ulrich, A., Baumann, W. 1999. Hydrological and geochemical factors affecting leachate composition in municipal solid waste incinerator bottom ash: Part II. The geochemistry of leachate from Landfill Lostorf, Switzerland, J. Contam. Hydrol. 40, 239-259.

Kosson, D.S. , van der Sloot, H.A. , Eighmy, T.T, 1996. An approach for estimation of contaminant release during utilization and disposal of municipal waste combustion residues, J. Hazard. Mat. 47, 43-75.

Lidelöw, S., Lagerkvist, A., 2007. Evaluation of leachate emissions from crushed rock and municipal solid waste incineration bottom ash used in road construction, Waste Manage. 27, 1356-1365.

Meima, J.A., Comans, R.N.J., 1997. Geochemical modeling of weathering reactions in municipal solid waste incinerator bottom ash, Environ. Sci. Technol. 31, 1269-1276.

Mostbauer P., Lechner P., 2006. Weathering of MSWI bottom ash in laboratory test cells and under field conditions - Effect on metal and metalloid mobility. WASCON 2006 conference proceedings, Belgrade (Serbia).

Park, J.Y., Batchelor, B., 2002. A multi-component numerical leach model coupled with a general chemical speciation code, Water Res. 36, 156-166.

Perkins, R., Palmer, C., 1999. Solubility of ettringite ($Ca_6[Al(OH)_6]_2(SO_4)_3 \cdot 26H_2O$) at 5-75°C. Geochim. Cosmochim. Ac. 63, 1969-1980.

Piantone, P., Bodénan, F., Chatelet-Snidaro, L., 2004. Mineralogical study of secondary mineral phases from weathered MSWI bottom ash: implications for the modelling and trapping of heavy metals, Appl. Geochem. 19, 1891-1904.

Rendek, E., Ducom, G., Germain, P. (2006). Influence of organic matter on municipal solid waste incinerator bottom ash carbonation, Chemosphere 64, 1212-1218.

Schmidt, T., Lothenbach, B., Romer, M., Scrivener, K., Rentsch, D., Figi, R., 2008. A thermodynamic and experimental study of the conditions of thaumasite formation, Cement Concrete Res. 38, 337-349.

Speiser, C., Baumann, T., Niessner, R., 2000. Morphological and chemical characterization of calcium-hydrate phases formed in alteration processes of deposited municipal solid waste incinerator bottom ash, Environ. Sci. Technol. 34, 5030-5037.

Stronach, S.A., Glasser, F.P., 1997. Modeling the impact of abundant geochemical components on phase stability and solubility of the CaO-SiO_2-H_2O systems at 25°C: Na^+, K^+, SO_4^{2-}, Cl^- and CO_3^{2-}. Adv. Cem. Res. 9, 167-181.

Suer, P., Lindqvist, J.E., Arm, M., Frogner-Kockum, P., 2009. Reproducing ten years of road ageing — Accelerated carbonation and leaching of EAF steel slag, Sc. Total Environ. 407, 5110-5118.

van der Lee, J., De Windt, L., Lagneau, Goblet, P., 2003. Module-oriented modeling of reactive transport with HYTEC. Comput. Geosci. 29, 265-275.

van Zoemeren, A., Comans, R. N. J., 2004. Contribution of natural organic matter to copper leaching from municipal solid waste incinerator bottom ash, Environ. Sc. Technol. 38, 3927–3932.

Wolery, T., 1992. EQ3/6. A software package for geochemical modelling of aqueous systems: package overview and installation guide (version 7.0). Technical Report UCRL-MA-110662 PT I ed., Lawrence Livermore National Laboratory, USA.

Table 1. Thermodynamic equilibrium constants of the solid phases considered in the calculation of saturation indices and the reactive transport modeling.

Mineral	Reaction of formation	LogK 0 °C	25 °C	Ref.
Amorphous $Al(OH)_3$	$Al^{3+} + 3\ H_2O \rightarrow Al(OH)_3\ (am) + 3\ H^+$	-12.2	-10.4	[a]
Calcite	$Ca^{2+} + CO_3^{2-} \rightarrow CaCO_3$	8.4	8.5	[a]
C-S-H 0.8	$0.8\ Ca^{2+} + H_4SiO_4 - 0.4\ H_2O \rightarrow$ C-S-H 0.8 $+ 1.6\ H^+$	-	-11.1	[b]
C-S-H 1.1	$1.1\ Ca^{2+} + H_4SiO_4 + 0.2\ H_2O \rightarrow$ C-S-H 1.1 $+ 2.2\ H^+$	-	-16.7	[b]
C-S-H 1.8	$1.8\ Ca^{2+} + H_4SiO_4 + 1.6\ H_2O \rightarrow$ C-S-H 1.8 $+ 3.6\ H^+$	-	-32.6	[b]
Ettringite	$2\ Al^{3+} + 6\ Ca^{2+} + 3\ SO_4^{2-} + 38\ H_2O \rightarrow Ca_6Al_2(SO_4)_3(OH)_{12}{:}26H_2O + 12\ H^+$	-63.3	-56.9	[c,d]
Foshagite	$4\ Ca^{2+} + 3\ H_4SiO_4 - H_2O \rightarrow Ca_4Si_3O_9(OH)_2 + 8\ H^+$	-71.4	-65.9	[d]
Friedel's salt	$4\ Ca^{2+} + 2\ Al^{3+} + 2\ Cl^- + 12\ H_2O \rightarrow Ca_4Al_2Cl_2(OH)_{12}{:}4H_2O + 12\ H^+$	-73	-63.8	[e]
Gehlenite	$2\ Ca^{2+} + 2\ Al^{3+} + H_4SiO_4 + 3\ H_2O \rightarrow Ca_2Al_2SiO_7 + 10\ H^+$	-64.6	-56.8	[a]
Gibbsite	$Al^{3+} + 3\ H_2O \rightarrow Al(OH)_3 + 3\ H^+$	-10.3	-8.8	[a]
Gypsum	$Ca^{2+} + SO_4^{2-} + 2\ H_2O \rightarrow CaSO_4{:}2H_2O$	4.9	4.8	[a]
Halite	$Na^+ + Cl^- \rightarrow NaCl$	-1.5	-1.6	[a]
Hillebrandite	$2\ Ca^{2+} + H_4SiO_4 + H_2O \rightarrow Ca_2(OH)_2SiO_3 + 4\ H^+$	-40.0	-36.8	[d]
Monosulfoaluminate	$2\ Al^{3+} + 4\ Ca^{2+} + SO_4^{2-} + 12\ H_2O \rightarrow Ca_4Al_2SO_4(OH)_{12} + 12\ H^+$	-	-73.0	[f]
Monohydrocalcite	$Ca^{2+} + CO_3^{2-} + H_2O \rightarrow CaCO_3{:}H_20$	7.6	7.7	[d]
Pseudo-wollastonite	$Ca^{2+} + H_4SiO_4 - H_2O \rightarrow CaSiO_3 + 2\ H^+$	-15.3	-13.9	[a]
Portlandite	$Ca^{2+} + 2\ H_2O \rightarrow Ca(OH)_2 + 2\ H^+$	-24.7	-22.7	[a]
Quartz	$H_4SiO_4 \rightarrow SiO_2 + 2\ H_2O$	4.4	4.0	[a]
Sylvite	$K^+ + Cl^- \rightarrow KCl$	-0.5	-0.9	[d]
Thaumasite	$6\ Ca^{2+} + 2\ H_4SiO_4 + 2\ CO_3^{2-} + 2\ SO_4^{2-} + 28\ H_2O \rightarrow Ca_6(SiO_3)_2O_{16}(CO_3)_2(SO_4)_2{:}30H_20 + 4\ H^+$	-67.0	-63.8	[g]
Tobermorite	$5\ Ca^{2+} + 6\ H_4SiO_4 - 2\ H_2O \rightarrow Ca_5Si_6O_{16}(OH)_2{:}4H_20 + 10\ H^+$	-67.0	-63.8	[d]
Anglesite	$Pb^{2+} + SO_4^{2-} \rightarrow PbSO_4$	7.9	7.8	[a]
Barite	$Ba^{2+} + SO_4^{2-} \rightarrow BaSO_4$	10.4	10.0	[a]
Cerussite	$Pb^{2+} + CO_3^{2-} \rightarrow PbCO_3$	13.5	13.1	[a]
$Cu(OH)_2$	$Cu^{2+} + 2\ H_2O \rightarrow Cu(OH)_2 + 2\ H^+$	-9.7	-8.6	[a]
Hydrocerussite	$3\ Pb^{2+} + 2\ CO_3^{2-} + 2\ H_2O \rightarrow Pb_3(CO_3)_2(OH)_2 + 2\ H^+$	-	17.5	[a]
Malachite	$2\ Cu^{2+} + CO_3^{2-} + 2\ H_2O \rightarrow Cu_2CO_3(OH)_2 + 2\ H^+$	4.1	5.2	[a]
$Pb(OH)_2$	$Pb^{2+} + 2\ H_2O \rightarrow Pb(OH)_2 + 2\ H^+$	-	-11.0	[h]
$Pb_2(OH)_3Cl$	$2\ Pb^{2+} + Cl^- + 3\ H_2O \rightarrow Pb_2(OH)_3Cl + 3\ H^+$	-	-8.8	[a]
Tenorite	$Cu^{2+} + H_2O \rightarrow CuO + 2\ H^+$	-8.7	-7.6	[a]
Witherite	$Ba^{2+} + CO_3^{2-} \rightarrow BaCO_3$	8.6	8.6	[a]

[a] MINTEQ, Allison et al. (1991), [b] fit from Stronach and Glasser (1997), [c] Perkins and Palmer (1999), [d] EQ3/6, Wolery (1992), [e] Bothe and Brown (2004), [f] Damidot and Glasser (1993),[g] Schmidt et al. (2008), [h]Adjusted, see De Windt and Badreddine(2007).

Table 2.
Transport parameters used in the reactive transport calculations.

	Hydraulic conductivity K [m/s]	Pore diffusion coefficient D_p [m^2/s]	Effective porosity ω [%]
Hérouville			
Asphalt cover	$2x10^{-7}$	-	-
BA subbase	$5x10^{-6}$	10^{-10}	30
BA pathway (geomembrane)	10^{-3}	10^{-9}	30
Dåva			
Asphalt cover	$5x10^{-6}$	-	-
Gravel and sand	10^{-5}	10^{-9}	30
BA subbase	$5x10^{-6}$	10^{-9}	30

Table 3.
Calculated saturation indices (SI) for a selection of leachates representative of successive weathering stages (the solid phases considered in the reactive transport modeling are in bold).

	Hérou-ville				Dåva (slope)				Dåva (pav.)
Time	+7 d	+250 d	+3 y	+10 y	+13 d	+250 d	+3 y	+6 y	+3y
Temp. [°C]	22	18	17	19	12	24	12	15	8
pH	12.4	11.4	8.3	7.6	11.1	10.7	11.1	7.8	10.8
Cement-type phases									
C-S-H 0.8	-0.6	-0.3	-4.0	-5.1	-	-	-	-5.7	-
C-S-H 1.1	0.8	0.2	-5.5	-7.0	-	-	-	-7.5	-
C-S-H 1.8	0.8	-1.5	-11.9	-14.2	-	-	-	-14.5	-
Tobermorite	4.7	4.2	-4.0	-26.7	-	-	-	-30	-
(1)	(0.8)	(0.7)	(-0.7)	(-4.5)				(-5)	
Foshagite	1.6	-2.5	-25	-29.5	-	-	-	-31.5	-
(1)	(0.5)	(-0.8)	(-8.3)	(-9.8)				(-10.5)	
Hillebrandite	0.6	-2.5	-14.4	-16.6	-	-	-	17.3	-
Thaumasite	3.1	-7.4	-21.4	-9.2	-	-	-	-13.8	-
Ettringite	6.3	0.1	-14.5	-16.7	1.5	-2.6	-0.1	-18.6	-2.8
Monosulfoal.	1.4	-4.8	-19.4	-22.6	-4.7	-6.1	-5.3	-23.4	-8.4
Friedel's salt	2.3	-2.6	-17.5	-23.5	2.1	-5.4	-3.1	-21.1	-1.9
Portlandite	-0.3	-2.9	-9.7	-10.5	-4.3	-4.8	-4.4	-10.7	-5.9
Other phases (major elements)									
$Al(OH)_3$(am)	-3.9	-3.0	0.0	-0.5	-1.0	0.6	-0.8	-0.4	-0.1
Calcite	-	-	-	0.1	1.0	-	1.2	-0.9	0.8
Monohydrocalc.	-	-	-	-0.7	0.2	-	0.4	-1.7	0.0
Gehlenite	-6.4	-7.7	-14	-17.2	-	-	-	-17.7	-
Gibbsite	-2.2	-1.3	1.7	1.1	0.8	0.9	0.9	1.3	1.7
Gypsum	-0.9	-1.1	-1.3	-0.6	-0.9	-1.5	-1.4	-1.5	-1.5
P-Wollastonite	1.2	0.7	-4.5	-5.7	-	-	-	-6.4	-
Quartz	-3.3	-1.3	0.4	0.1	-	-	-	-0.6	-
Other phases (trace elements)									
Barite	-	-	-	-	0.4	-0.1	0.4	0.4	0.6
Witherite	-	-	-	-	-2.9	-	-2.2	-4.1	-2.3
Anglesite	-9.7	-7.8	-3.2	-4.6	-8.4	-7.4	-8.4	-5.5	-7.3
Cerussite	-	-	-	-2.1	-4.8	-	-3.9	-3.2	-3.1
Hydrocerussite	-	-	-	-7.7	-9.8	-	-7.7	-9.8	-6.1
Litharge	-1.9	-2.3	-4.3	-7.5	-4.4	-3.5	-4.0	-7.5	-4.1
$Pb(OH)_2$(s)	-0.1	0.2	-2.1	-5.4	-2.1	-1.7	-1.7	-5.3	-1.5
$Pb_2(OH)_3Cl$	-1.1	-0.8	-1.7	-8.2	-2.7	-2.4	-4.4	-7.8	-2.3
$Cu(OH)_2$[(2)]	1.0	0.4	-0.5	-0.8	0.1	0.0	-0.9	-1.8	0.0
Malachite[(2)]	-	-	-	0.4	-3.9	-	-5.2	-2.7	-2.7
Tenorite[(2)]	2.1	1.6	0.5	0.2	1.0	1.0	0.2	-0.7	1.0

(1) Normalized to 1 atom of Si for comparison with the other C-S-H phases. (2) The interaction between Cu and the dissolved organic matter is not taken into account for the SI calculations.

Table 4.

Initial mineralogical content of the MSWI BA considered for the batch and reactive transport modeling.

	Hérouville [wt.%(1)]	Dåva [wt.%]		Hérouville [wt.%]	Dåva [wt.%]
Calcite	10	10	Halite	0.28	0.35
Hillebrandite or P-wollastonite	2.5	-	Portlandite	1	-
Tobermorite or P-wollastonite	-	2.5	Sylvite	0.08	0.05
Ettringite	1	1	Litharge	0.1	0.1
Gypsum	0.05	0.05	Tenorite	0.1	0.1

(1) wt% of dried MSWI BA.

Figure captions

Fig. 1 Schematic representation of the two pilot-scale roads and modeling grids with the sampling collectors marked by the symbol ⊗. Due to symmetry, half a cross section is sufficient for the Dåva grid. The black upper boundary condition of rainwater infiltration and the grid nodes in white are used to simulate the partial runoff of rainwater at the surface.

Fig. 2. Plot of the leachate experimental data on SO_4 and Al solubility diagrams calculated at 25 °C for conditions representative of the leachate (Hérouville: tot. $Al^{3+} = 3x10^{-5}$, tot. $Ca^{2+} = 2.5x10^{-3}$, tot. $SO_4^{2-} = 1x10^{-3}$; Dåva: tot. $Al^{3+} = 1x10^{-4}$, tot. $Ca^{2+} = 1x10^{-3}$, tot. $SO_4^{2-} = 1x10^{-3}$). In the Dåva case the symbols ○ and ● stand for leachate collector under the slope and the road, respectively.

Fig. 3. Experimental and modeling data of batch tests applied to the Hérouville and Dåva MSWI bottom ashes.

Fig. 4. Calculated average annual Darcy flow and Cl concentration profiles after 3 years of leaching. The upper vectors correspond to water runoff at the surface of the asphalt towards the soil (Hérouville) or the ditch (Dåva).

Fig. 5. Evolution with time of the leachante concentrations of elements and dissolved organic carbon at the sampling points. The saturation indices of the leachates surrounded by the square symbols are reported in Table 3.

Fig. 6. Evolution with time of leachate pH at the sampling points assessing temperature effect and CO_2 inputs. The saturation indices of the leachates surrounded by the square symbol are reported in Table 3.

Fig. 7. Evolution with time of major element concentrations in the leachates at the sampling points assessing temperature effect, CO_2 inputs and mineralogical variants of the model. The saturation indices of the leachates surrounded by the square symbol are reported in Table 3.

Fig. 8. Calculated mineralogical evolution of the MSWI bottom ashes close to the sampling point at Hérouville. Left: evolution with time of the pH-buffering minerals. Right: transformation of ettringite into calcite, gypsum and aluminum hydroxide.

Fig. 9. Evolution with time of Ba, Cu and Pb concentrations in the leachates at the sampling points assessing temperature effect and Cu complexation by dissolved organic matter. The saturation indices of the leachates surrounded by the square symbol are reported in Table 3.

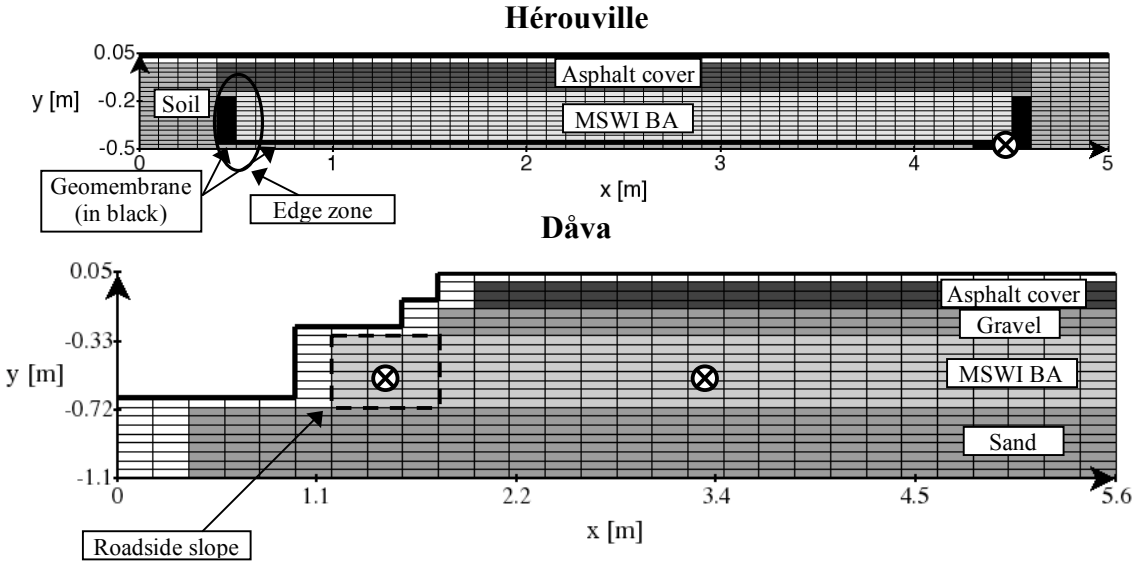
Hérouville
0.05
-0.2
-0.5
y [m]
Soil
Asphalt cover
MSWI BA
0
1
2
3
4
5
x [m]
Geomembrane
(in black)
Edge zone
Dåva
0.05
-0.33
-0.72
-1.1
y [m]
Asphalt cover
Gravel
MSWI BA
Sand
0
1.1
2.2
3.4
4.5
5.6
x [m]
Roadside slope

Figure 1

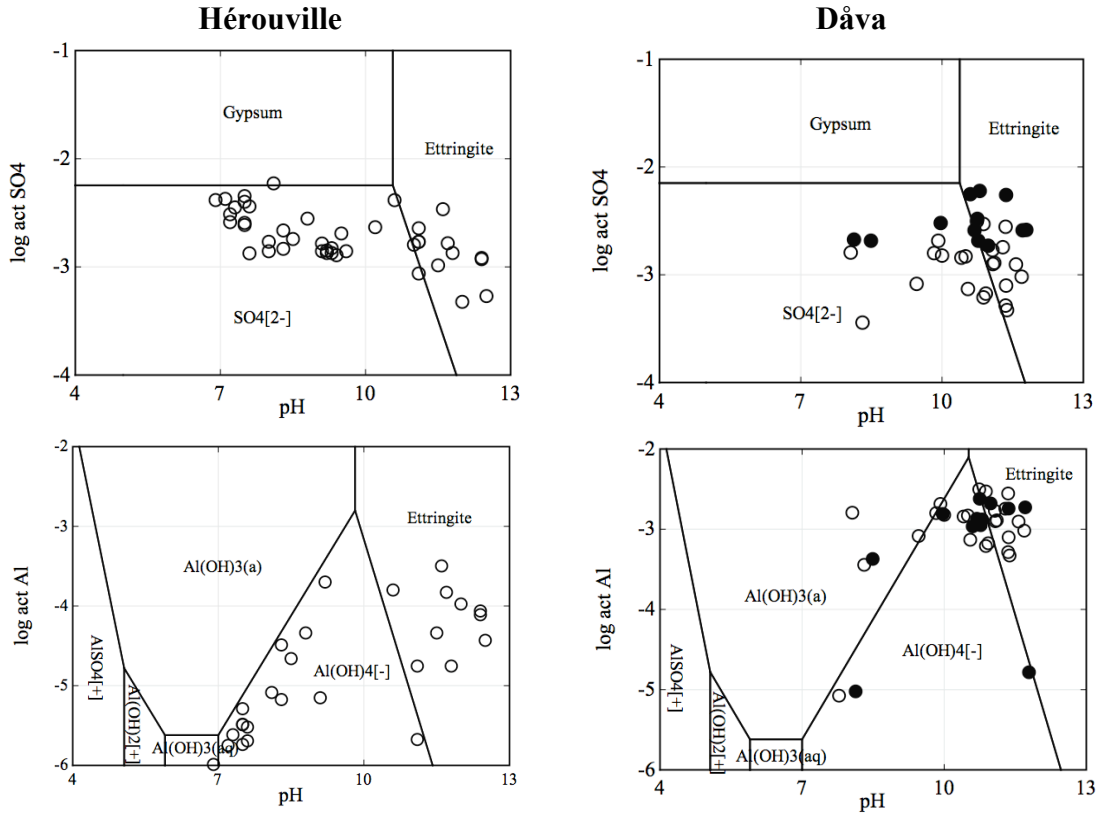
Hérouville
Dåva
log act SO4
Gypsum
Ettringite
SO4[2-]
pH
log act Al
Al(OH)3(a)
Al(OH)4[-]
AlSO4[+]
Al(OH)2[+]
Al(OH)3(aq)

Figure 2

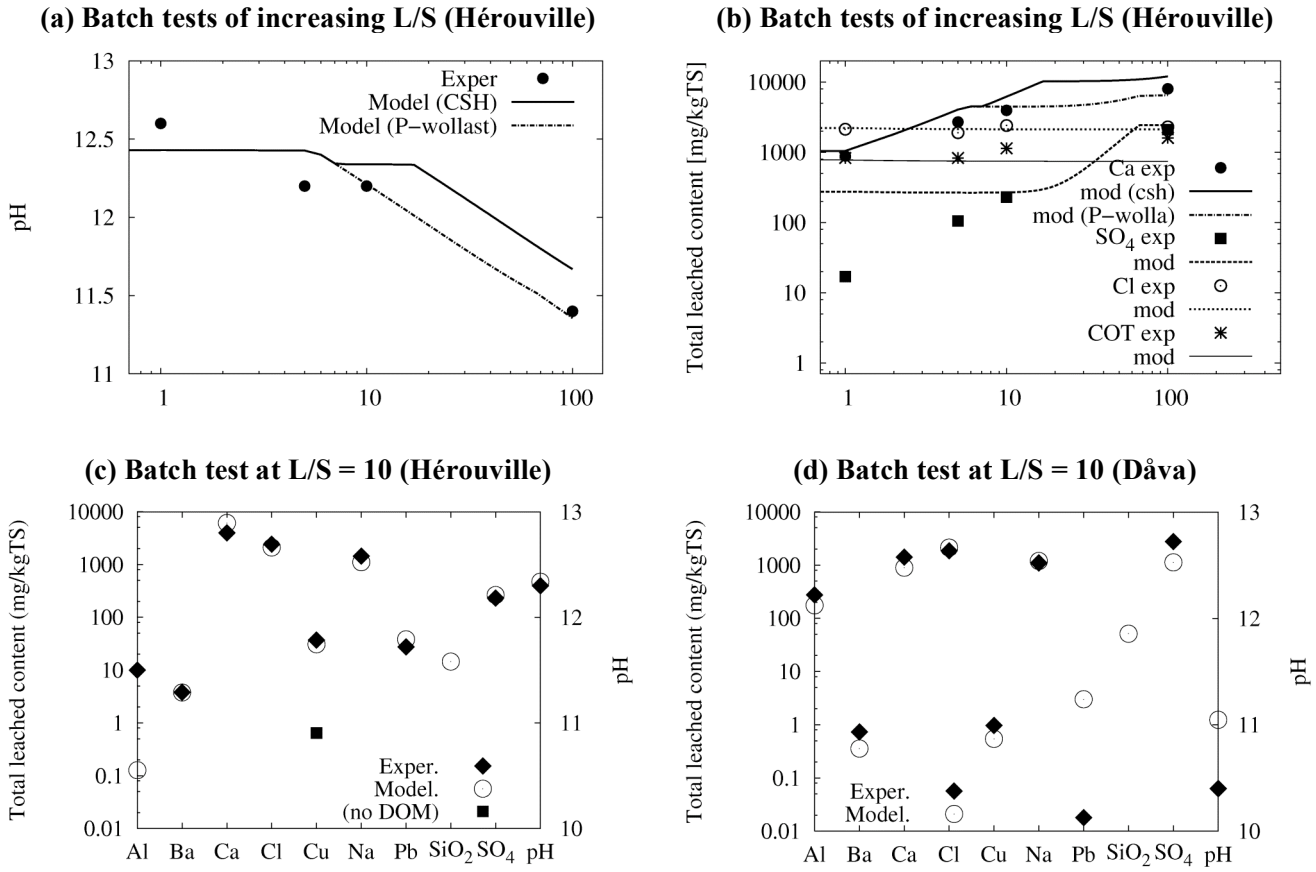
(a) Batch tests of increasing L/S (Hérouville)
pH
Exper
Model (CSH)
Model (P−wollast)
(b) Batch tests of increasing L/S (Hérouville)
Total leached content [mg/kgTS]
Ca exp
mod (csh)
mod (P−wolla)
SO4 exp
mod
Cl exp
mod
COT exp
mod
(c) Batch test at L/S = 10 (Hérouville)
Total leached content (mg/kgTS)
pH
Exper.
Model.
(no DOM)
Al Ba Ca Cl Cu Na Pb SiO2 SO4 pH
(d) Batch test at L/S = 10 (Dåva)
Total leached content (mg/kgTS)
pH
Exper.
Model.
Al Ba Ca Cl Cu Na Pb SiO2 SO4 pH

Figure 3

Hérouville

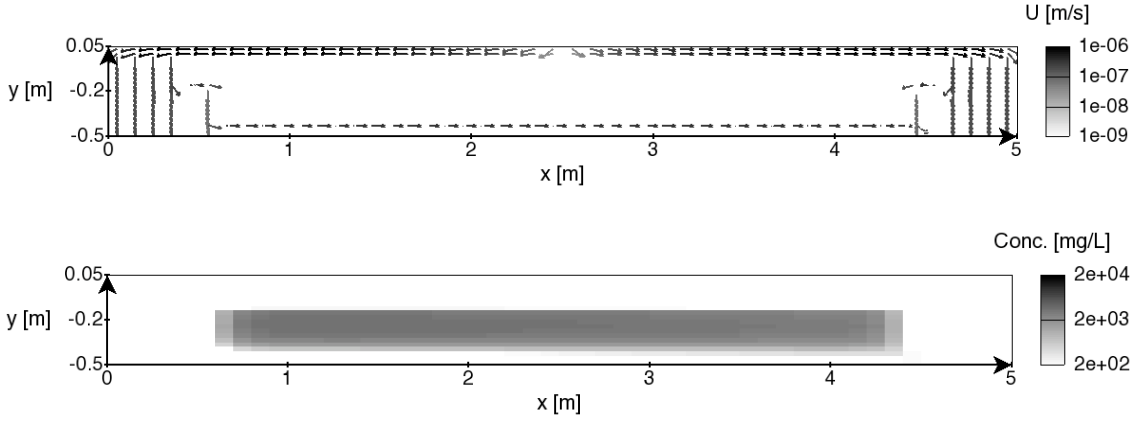

Dåva

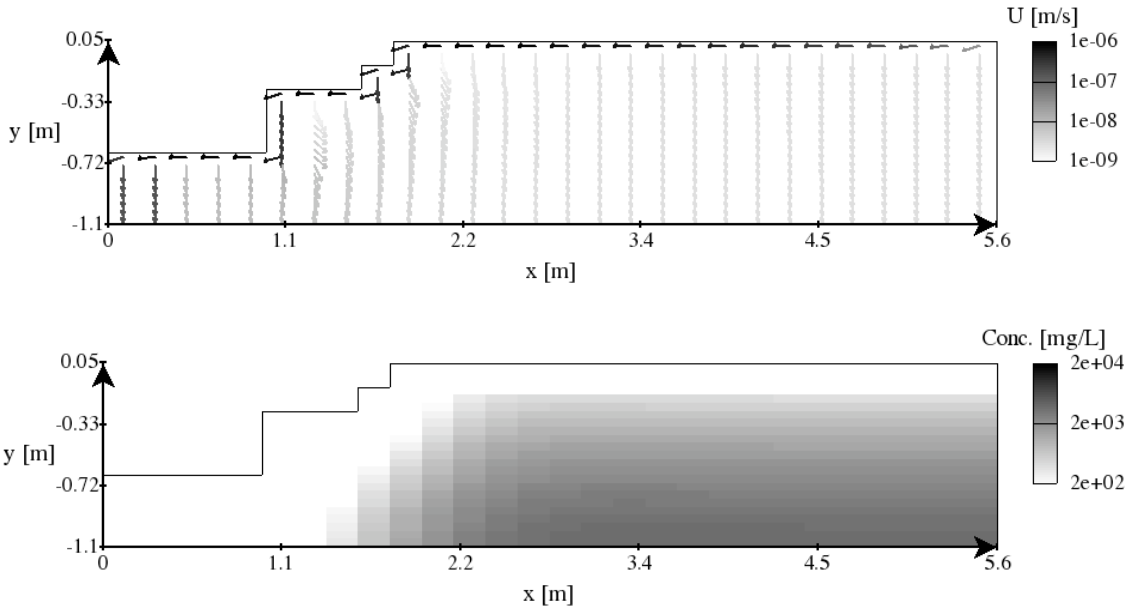

Figure 4

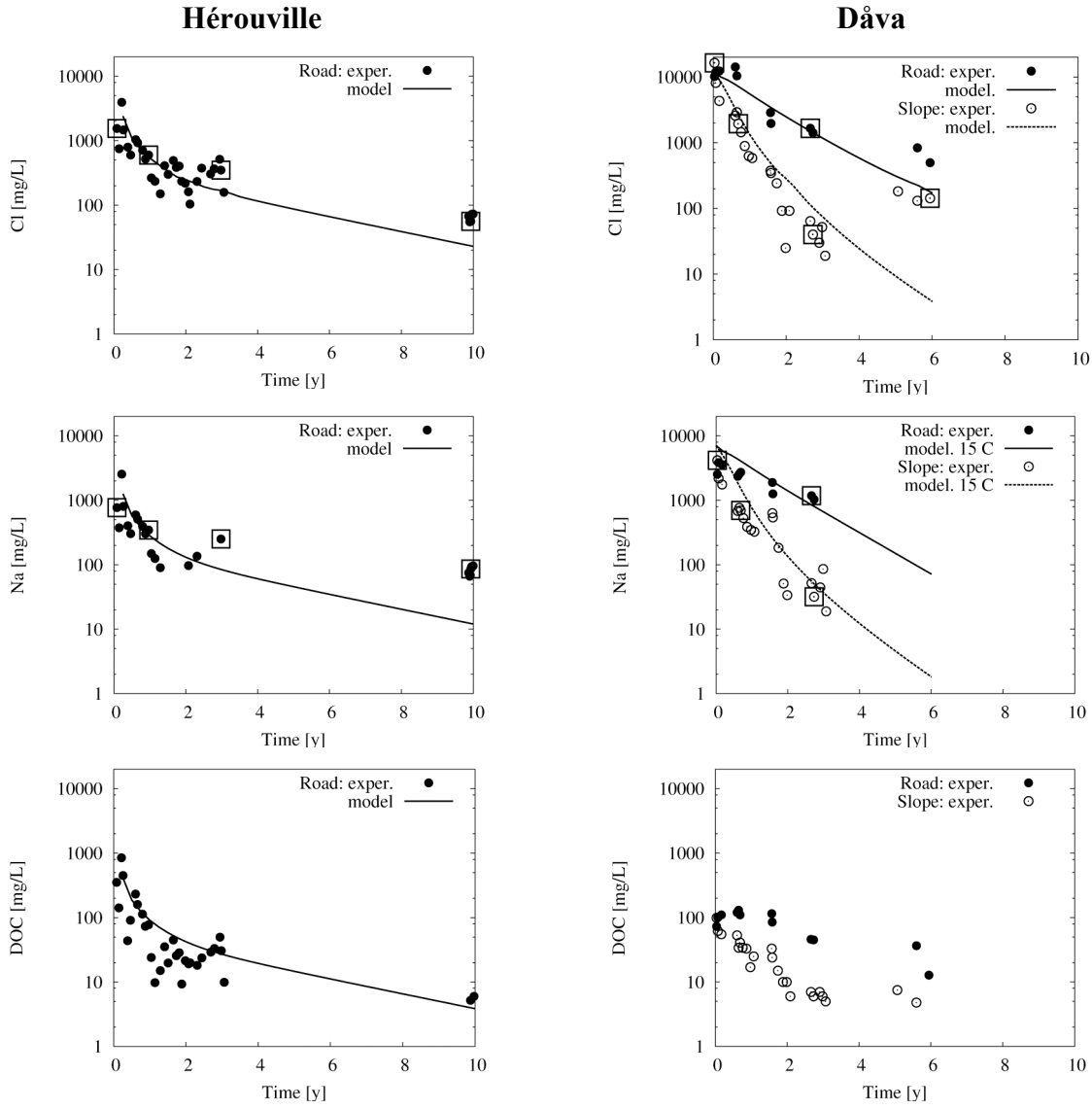
Hérouville
Dåva
Cl [mg/L]
Na [mg/L]
DOC [mg/L]
Time [y]
Road: exper.
model
Slope: exper.
model.
model. 15 C

Figure 5

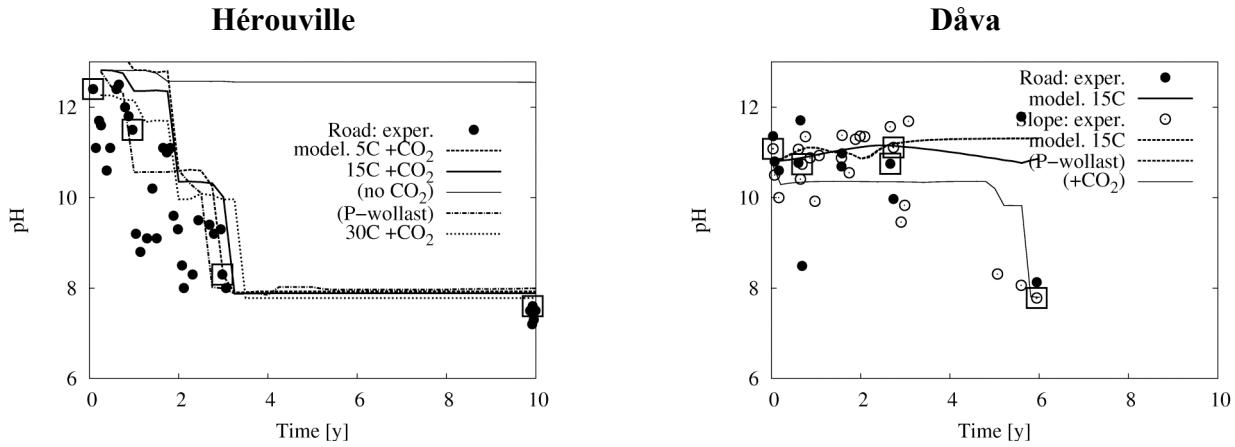
Hérouville
Dåva
pH
Time [y]
Road: exper.
model. 5C +CO2
15C +CO2
(no CO2)
(P−wollast)
30C +CO2
Slope: exper.
model. 15C
(P−wollast)
(+CO2)

Figure 6

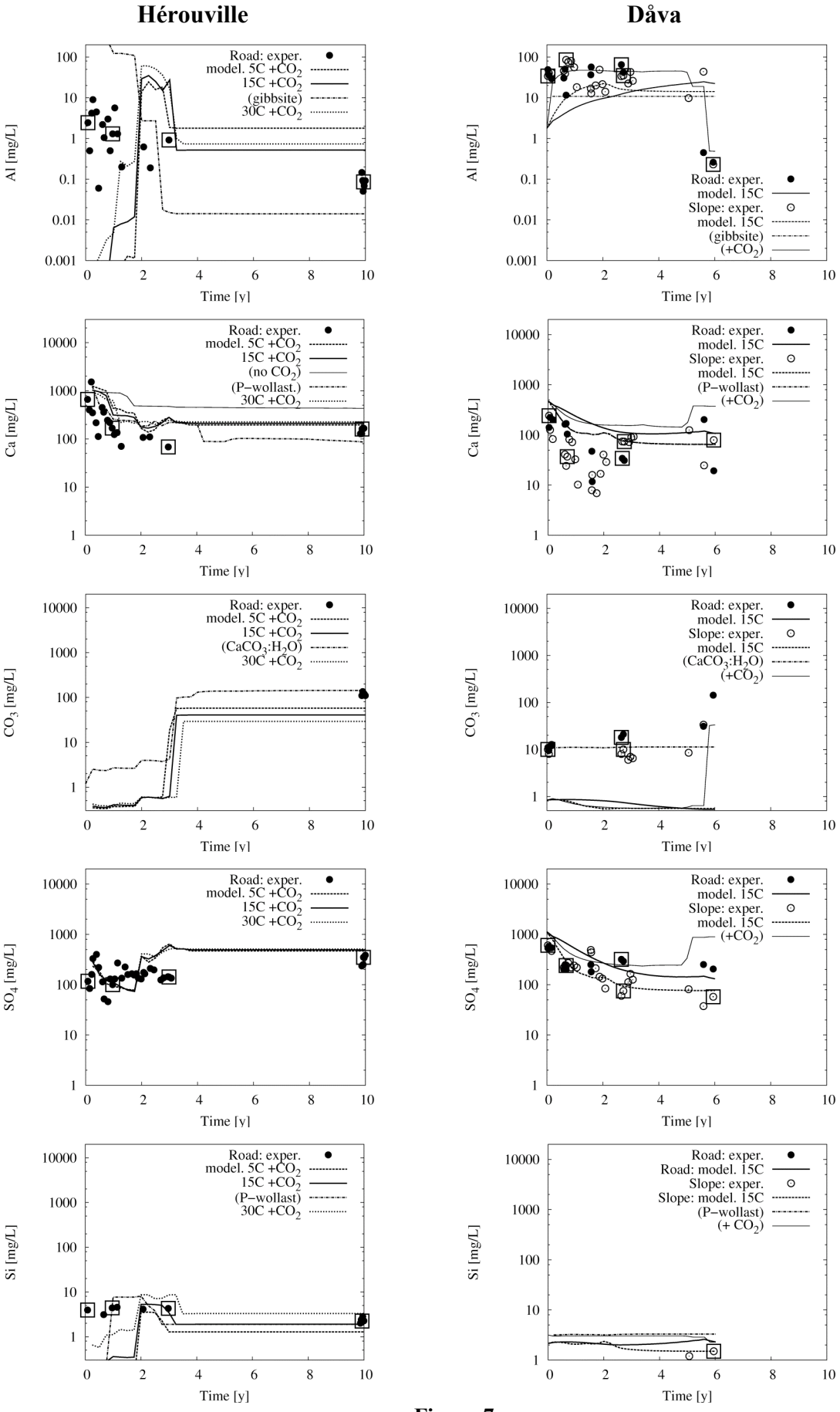
Hérouville
Dåva
Al [mg/L]
Ca [mg/L]
CO_3 [mg/L]
SO_4 [mg/L]
Si [mg/L]
Time [y]
Road: exper.
model. 5C +CO_2
15C +CO_2
(gibbsite)
30C +CO_2
Slope: exper.
model. 15C
(+CO_2)
(no CO_2)
(P−wollast.)
(P−wollast)
($CaCO_3$:H_2O)
Road: model. 15C
Slope: model. 15C
(+ CO_2)

Figure 7

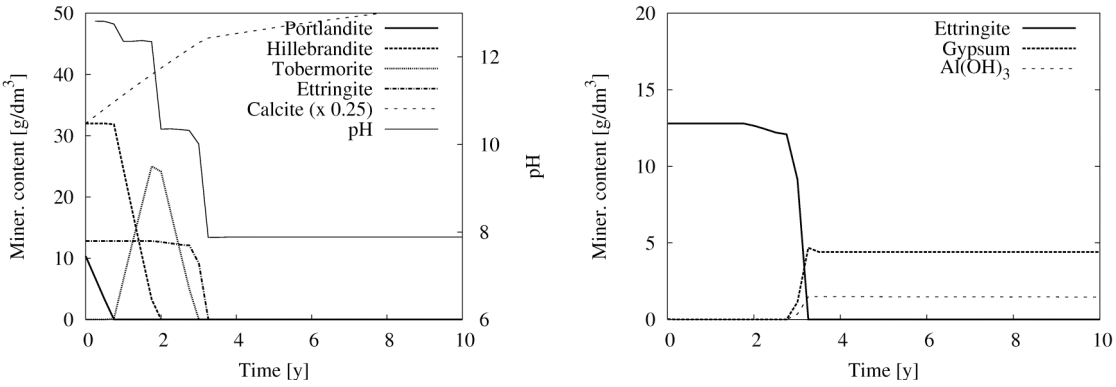
Portlandite
Hillebrandite
Tobermorite
Ettringite
Calcite (x 0.25)
pH
Miner. content [g/dm3]
pH
Time [y]
Ettringite
Gypsum
Al(OH)3
Miner. content [g/dm3]
Time [y]

Figure 8

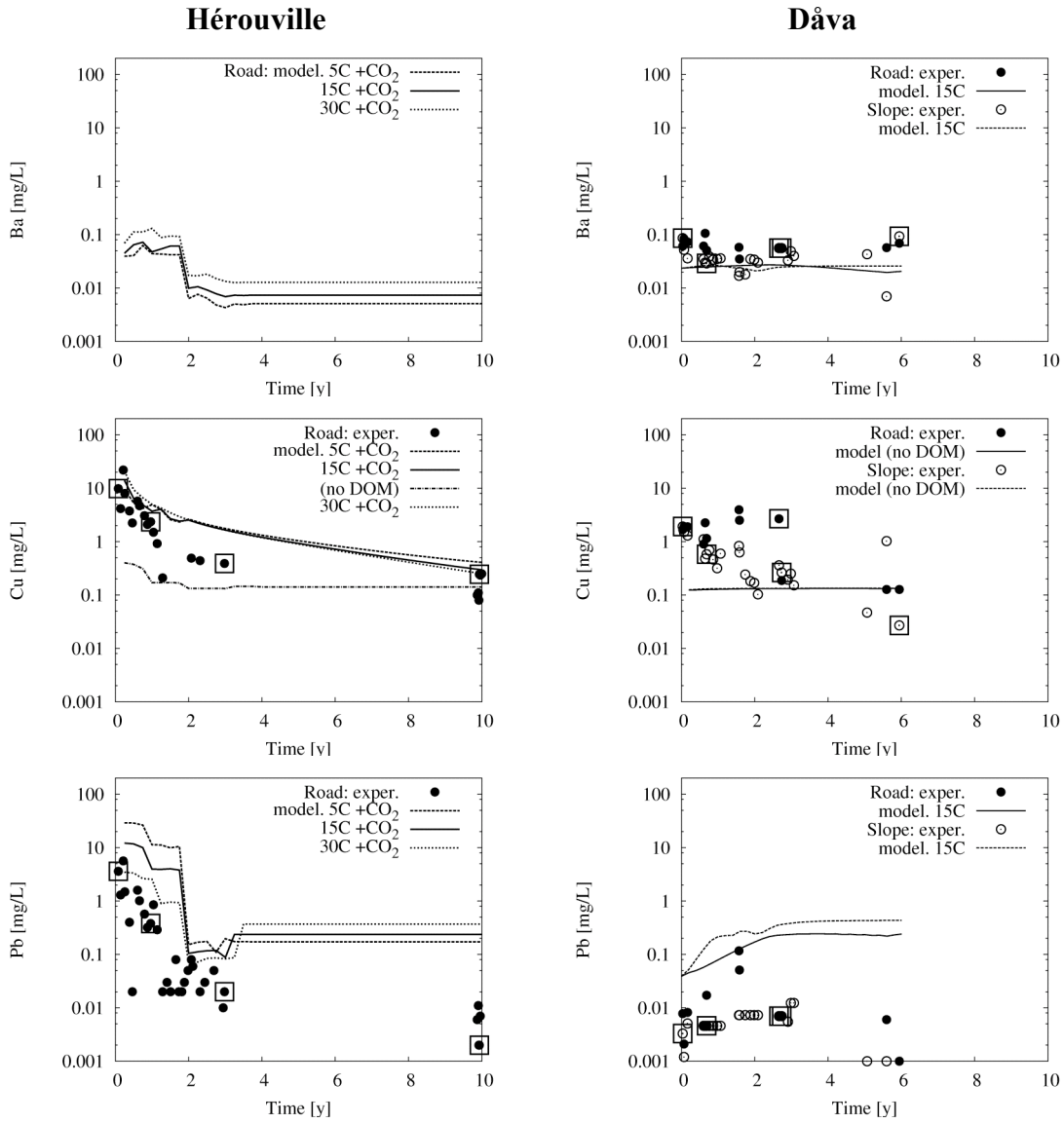
Hérouville
Dåva
Ba [mg/L]
Cu [mg/L]
Pb [mg/L]
Time [y]
Road: model. 5C +CO2
15C +CO2
30C +CO2
Road: exper.
model. 5C +CO2
15C +CO2
(no DOM)
30C +CO2
model. 15C
Slope: exper.
model (no DOM)

Figure 9